

## New vibration control device and analytical method for slender structures

Hideo Takabatake\* and Fumiya Ikarashi

*Department of Architecture, Kanazawa Institute of Technology, Institute of Disaster and Environmental Science  
3-1, Yatsukaho, Hakusan City, Ishikawa 924-0838, Japan*

*(Received July 15, 2011, Revised December 28, 2011, Accepted February 14, 2012)*

**Abstract.** Since slender structures such as utility poles, radio masts, and chimneys, are essentially statically determinate structures, they often collapse during earthquakes. Although vibration control is the most logical method for improving the earthquake resistance of such structures, there are many practical problems with its implementation due to their very long natural vibration period. This paper proposes a new vibration control device to effectively prevent the collapse of slender structures subjected to strong earthquakes. The device consists of a pendulum, an elastic restraint and a lever, and is designed such that when it is attached to a slender structure, the second vibration mode of the structure corresponds to the first vibration mode of the same structure without the device attached. This is highly effective in causing the transverse motions of the device and the structure to oppose each other and so reduce the overall transverse vibration during an earthquake. In the present paper, the effectiveness of the vibration control device is first evaluated based on laboratory experiments and numerical studies. An example of applying the device to a tall chimney is then simulated. A new dynamic analytical method for slender structures with abrupt rigidity variations is then proposed.

**Keywords:** slender structure; vibration control; vibration control device; long period; pendulum type; earthquake resistance; dynamic analyses; abrupt variation of rigidity.

---

### 1. Introduction

Slender structures such as utility poles, emergency radio masts, chimneys, and towers essentially behave as cantilevers when subjected to external loads. Since such structures often play important public roles, there is a need to improve their resistance to collapse due to severe earthquake ground motion. These structures are particularly influenced by long-period earthquake waves because they naturally have long vibration periods. The most common failure mechanism is for the structure to fall over due to the overturning moment, thus losing all functionality. Due to the importance of guarding against such failure, many vibration control methods have been considered in order to reduce the response of the structure to external loads.

Vibration control methods for general structures can be broadly divided into three categories: passive control, semi-active control and active control. Table 1 demonstrates various vibration

---

\*Corresponding author, Professor & Director, E-mail: [hideo@neptune.kanazawa-it.ac.jp](mailto:hideo@neptune.kanazawa-it.ac.jp)

Table 1 Previously proposed vibration control devices

<b>Passive control device</b>		
TMD (TVA)	Tuned Mass Dampers (Tuned Vibration Absorber)	Chang and Soong (1980), Thompson (1981), Kaynia <i>et al.</i> (1981), Abé (1996), Tesar (1999), Sun <i>et al.</i> (1995)
PTMD	Pendulum Tuned mass Damper	Gerges and Vickery (2005), Takabatake and Satoh (2006), Roffel <i>et al.</i> (2011)
MTMD	Multiple Tuned Mass Dampers	Xu and Igusa (1992), Fujino and Abé (1993), Yamaguchi and Harnpornchai (1993), Igusa and Xu (1994), Abé and Fujino (1994)
MMD	Multiple Mass Dampers	Kareem and Kline (1995)
TM-MR	Tuned Masses Magnetorheological (MR) dampers	Zemp <i>et al.</i> (2011)
TLD	Tuned Liquid Dampers	Fujii <i>et al.</i> (1990)
LCD	Liquid Column Dampers	Ghosh and Basu (2004), Ghosh and Basu (2008)
TLCD	Tuned Liquid Column Dampers	Balendra <i>et al.</i> (1995), Won <i>et al.</i> (1996), Yalla and Kareem (2000)
<b>Semi-active control device</b>		
SA-TMD	Semi-Active Tuned Mass Dampers	Abé (1996), Abé and Igusa (1996), Nagarajaiah and Sonmez (2007)
SAF-TMD	Semi-Active Friction Tuned Mass Dampers	Lin <i>et al.</i> (2010)
SAIVS-TMD	Semi-Active Independently Variable Stiffness Tuned Mass Dampers	Nagarajaiah and Varadarajan (2004)
SAMPC	Semi-Active Multi-step Predictive Control with Magnetorheological (MR) dampers	Varadarajan and Nagarajaiah (2004), Setareh <i>et al.</i> (2007), Xu and Li (2008)
SAMPC-MR		
SAIVD	Semi-Active Independently Variable Dampers	Nagarajaiah and Narasimhan (2007)
<b>Active control device</b>		
ATMD	Active Tuned Mass Dampers	Chang and Soong (1980)
AVS	Active Variable Stiffness system	Kobori, <i>et al.</i> (1993)

control devices that have been previously proposed.

One of the most common passive control approaches is the use of tuned mass dampers (TMDs), which are generally designed to optimize the stiffness and damping coefficients. Chang and Soong (1980) studied the possibility of enhancing TMD effectiveness against wind action by the addition of an active control capability. Thompson (1981) considered optimization of the spring and damper rates of a dynamic vibration absorber. Kaynia *et al.* (1981) investigated the effectiveness of TMDs in the presence of seismic disturbances. Tesar (1999) demonstrated the applicability of TMDs to slender structures. Abé (1996) proposed a design method for TMDs for use on structures with bilinear hysteresis. Pendulum-type tuned mass systems, in particular, are widely used for slender structures for conventional vibration control. Gerges and Vickery (2005) investigated the optimum design of pendulum-type TMDs under dynamic loads due to both wind and earthquakes. Takabatake and Satoh (2006) demonstrated that vibration control is an effective means of reducing

the disagreeable swaying that occurs in super-high-rise buildings for extended periods following an earthquake. Roffel *et al.* (2011) developed a relatively simple vibration control design to compensate for the detuning that occurs in typical pendulum TMDs (PTMDs).

On the other hand, multiple TMDs (MTMDs), which consist of a large number of individual TMDs with natural frequencies distributed around the fundamental frequency of the structure, have been proposed as a means of compensating for the spread in natural vibration frequency due to the nonlinear rigidity of the target structure. Fujino and Abé (1993), Xu and Igusa (1992), Yamaguchi and Harnpornchai (1993), Igusa and Xu (1994), Abé and Fujino (1994) and Kareem and Kline (1995) showed that an MTMD is more robust against off-tuning than a conventional TMD with the same mass.

Either mass- or liquid-based systems can be used for vibration control of slender structures. Liquid systems offer the advantages of simplicity, as shown by Ghosh and Basu (2004), Ghosh and Basu (2008), Balendra *et al.* (1995), Won *et al.* (1996) and Yalla and Kareem (2000).

The weakest point concerning the above-mentioned passive control schemes is that they are incapable of responding with sufficient speed to the very rapid movement that occurs at the beginning of an earthquake. For this reason, semi-active control devices have been proposed by many researchers, as listed in Table 1.

The following restrictions apply to vibration control devices for slender structures. First, the device must be placed in a high position near the top of the structure where the cross-sectional area is very small. Second, when being applied to an existing structure, the device must be as light-weight as possible. Finally, since slender structures essentially behave as cantilevers, the dynamic behavior is mainly governed by elasticity.

Based on these considerations, vibration control for slender structures is usually only considered in terms of wind action as an external load. The additional mass of a TMD system that is effective in mitigating wind effects on general high-rise buildings is about 1% of the total mass of the original structure. However, a TMD system that is effective against earthquake excitations needs to be about 10% of the total mass. This means that the device itself must be large and, in the case of a slender structure, the structure may be excessively loaded. Since slender structures have a very large aspect ratio and are generally constructed with the standardized design structure even if the application purpose and setting place of them differ from each other, passive control devices are considered to be the most practical since they do not require any electrical equipment.

Therefore, the present paper proposes a new pendulum-type vibration control device for slender structures that improves on many of the weak points of previous pendulum-type devices. Such devices generally include systems based on shock absorption, pounding, and damping. However, for a device with a single compact mass, since the natural vibration period of the device must correspond to the long vibration period of the structure, it is necessary to make the rigidity of the strut supporting the mass extremely low. This means that when the strut is compressed it can easily buckle. If an alternative approach is used in order to avoid such buckling, such as hanging the mass from the strut, then there is a high risk of the mass colliding with the structure.

A large number of analytic studies have been carried out for slender structures without any abrupt rigidity variations. Static analyses for tapered members were performed by many researchers, such as Boley (1963), Takabatake (1990), Wang and Lee (1973), Rohde (1953), Prathap and Varadan (1976) and Gupta (1985, 1986). Takabatake and Mizuki (1995) reported a simplified dynamic analysis for a cantilevered, linearly tapered, thin-walled member with a discontinuous additional mass and/or structural rigidity, subjected to transverse vibrations.

However, structures in which abrupt rigidity variations occur, such as slender structures and

high-rise buildings with setbacks, cannot be directly solved numerically due to these rigidity changes. In such situations, the most effective analytical method is to separate the original structure at points where the abrupt rigidity variations occur and to use continuity conditions at the connecting points (Takabatake *et al.* 2011). For slender, one-dimensional structures, this involves ensuring continuity for displacement, rotation, bending moment, and shear force. However, this approach cannot be applied to structures with vibration control devices because the connection between the structure and the device represents an abrupt rigidity variation. A general analytical method that is applicable to such problems is still lacking.

The aims of the present study are twofold. First, a novel vibration control device is proposed that can prevent the collapse of slender structures during uncommonly large earthquakes. The effectiveness of the proposed device is evaluated both experimentally and numerically, and the finite element method (FEM) code SNAP is used to simulate the application of the proposed device to a tall steel chimney. Second, a general analytical method for slender structures with an abrupt rigidity variation at the joint between the structure and the vibration control device is proposed. This is based on converting the normal continuous rotation and bending moments at a connection point to new expressions using elastic restraints. This new concept is very effective for avoiding the analytical difficulties that normally arise due to abrupt rigidity variations. The numerical results indicate that this approach can be successfully applied to all cases involving rigidity variations.

## 2. New vibration control device

The vibration control device proposed here for slender structures satisfies the following advantages:

- (1) The idea is unique and free from existing licenses.
- (2) The same principle is applicable to various kinds of slender structures.
- (3) The weight of the device represents a small fraction of that of the structure.
- (4) Installation on existing structures is simple and fast.
- (5) The device does not disturb the original function of the structure.

The proposed device consists of a pendulum (I), an elastic restraint (II) and a lever (III), as

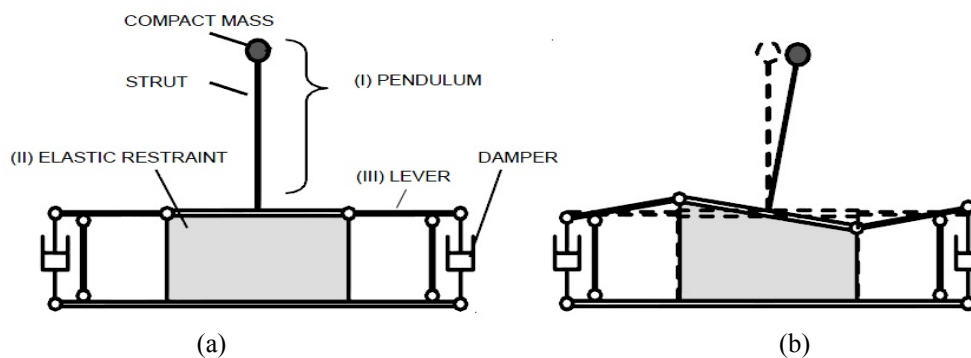


Fig. 1 Schematic illustration of proposed vibration control device: (a) functions and (b) state of vibration after the current capture

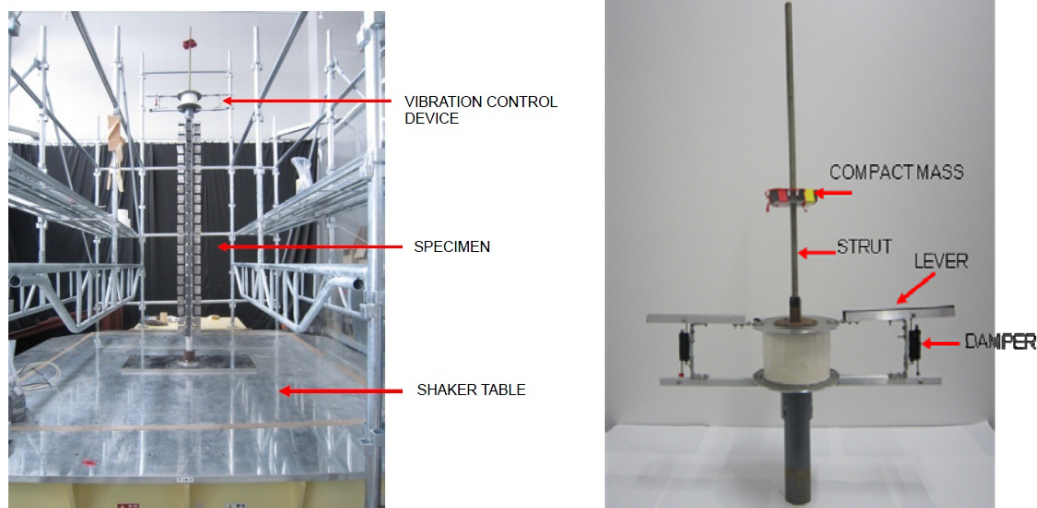
shown in Figs. 1 and 2(b). The function of the pendulum is to synchronize the vibration period of the device with the natural period of the structure by adjusting the weight and height of the compact mass. The elastic restraint increases the natural period of the pendulum by allowing it to rotate. This means that a pendulum strut with a high bending rigidity can be used in order to prevent buckling. The lever then transforms the relatively large vertical displacement of the elastic restraint to a smaller vertical displacement but more powerful vertical force of the rod connected to the damper (see Fig. 1), thus increasing the damping performance.

In addition, the proposed vibration control device is designed such that, when it is attached to a slender structure, the second vibration mode of the structure becomes identical to the first vibration mode of a structure without the device. This ensures that the motion of the pendulum directly opposes that of the structure, greatly reducing its response to earthquakes.

### 3. Experiment

#### 3.1 Experimental setup

The effectiveness of the proposed device was experimentally evaluated using a shaker table. Figs. 2(a) and (b) show photographs of the experimental setup and the vibration control device, respectively. The test specimen, representing a slender structure, was an aluminum tube (6063TD-H18) with a diameter of 0.06 m, a thickness of 0.002 mm and a height of 2 m. The values of Young's modulus and Poisson's ratio were  $683 \times 10^8 \text{ N/m}^2$  and 0.3, respectively. The specimen was free at the top and clamped at the base located on the shaker table. The shaker table oscillated in a single transverse direction. The vibration control device was set at the top of the specimen. In order to increase the vibration period of the specimen to correspond to that of a full-size structure, a large number of additional masses were attached to the specimen using angle



(a) Overall experimental setup

(b) Vibration control device

Fig. 2 Photographs of (a) overall experimental setup and (b) vibration control device

Table 2 Specimen parameters, natural periods, and damping constants

Specimen	Total height (m)	Vibration control device			Natural period (s)	Damping constant
		Diameter of elastic restraint (m)	Compact mass			
			Weight (kg)	Height (m)		
S2-0-0	2	Non	Non	Non	0.497	0.010
S2-0.15-0.45	2	φ0.15	0.45	0.60	0.496	0.045
S2-0.15-0.89	2		0.89	0.45	0.496	0.044
S2-0.20-4.04	2	φ0.20	4.04	0.60	0.496	0.040

Table 3 Maximum acceleration and velocity of earthquake input waveforms

No	Name	Original wave		Normalized wave	
		Maximum acceleration (m/s <sup>2</sup> )	Maximum velocity (m/s)	Maximum acceleration (m/s <sup>2</sup> )	Maximum velocity (m/s)
1	El Centro 1940 NS 50	3.42	0.33	5.11	0.50
2	JMA Kobe NS 50	8.18	0.91	4.50	0.50
3	Noto Peninsula EW 50	8.49	0.48	8.81	0.50
4	Tomakomai NS 50	0.69	0.30	1.16	0.50

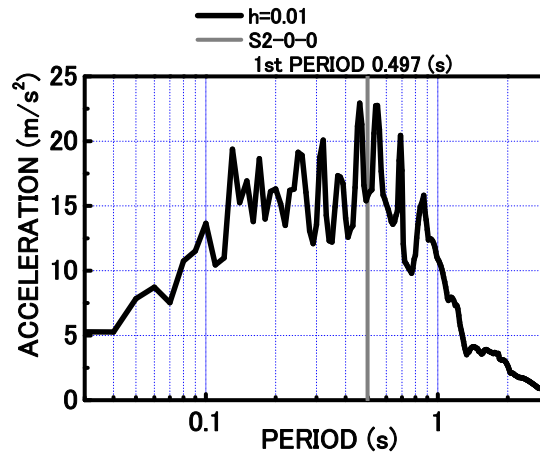


Fig. 3 Acceleration response spectrum for specimen S2-0-0, subjected to the El Centro 1940 NS 50 waveform

brackets placed along the longitudinal axis. The overall weight of the specimen thus changed from 2.16 to 90.96 kg. Four different experimental configurations were used, as shown in Table 2, where the three terms in the specimen name indicate the total height excluding the vibration control device, the diameter of the elastic restraint (urethane foam cylinder), and the weight of the

compact mass, respectively. S2-0-0 corresponds to a specimen without the vibration control device.

The height of the compact mass above the elastic restraint is set such that the second vibration mode for the specimen with the device corresponds to the first vibration mode for the specimen without the device. The damping constants for all specimens determined from the shaking tests are also shown in Table 2.

The fact that the experiments were carried out indoors placed strong restrictions on both the height and weight of the specimen. The weight of the vibration control device could not be reduced because it was constructed using commercially available components. In particular, the weight of the angle brackets used to set up the dampers was a sizeable fraction of the overall weight of the device. The ratio of the weight of the device to that of the specimen alone (90.96 kg) was 1/202, 1/102 and 1/32 for S2-0.15-0.45, S2-0.15-0.89 and S2-0.20-4.04, respectively. However, the ratio of the weight of the device is improved for practical slender structures because the weight of only the slender structure increases far greater than one of the vibration control device.

To examine the effectiveness of the proposed vibration control device, four different earthquake waveforms were used to vibrate the shaker table; these are described in Table 3. These acceleration waveforms were normalized to a maximum velocity of 0.5 m/s. Accelerations were measured using accelerometers installed at various points on the vibration control device and the specimen. Strains were measured by strain gauges mounted near the base of the specimen, and the bending moments and transverse shear forces were calculated from the measured strain values. Fig. 3 shows the acceleration response spectrum for specimen S2-0-0 (no vibration control) to the waveform for El Centro 1940 NS 50 with a damping constant of 0.01. It can be seen that the largest response occurs for a period of about 0.497 s, which is taken to be the natural vibration period for the specimen. Therefore, if the vibration control device is found to be effective against vibrations at this period, it can be considered highly successful.

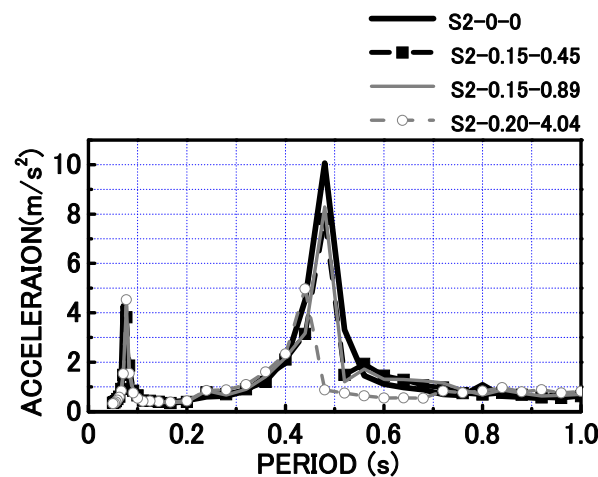


Fig. 4 Acceleration response spectrum at the top of specimens S2-0-0, S-0.15-0.45, S2-0.15-0.89, and S2-0.20-4.04, subjected to a sinusoidal waveform

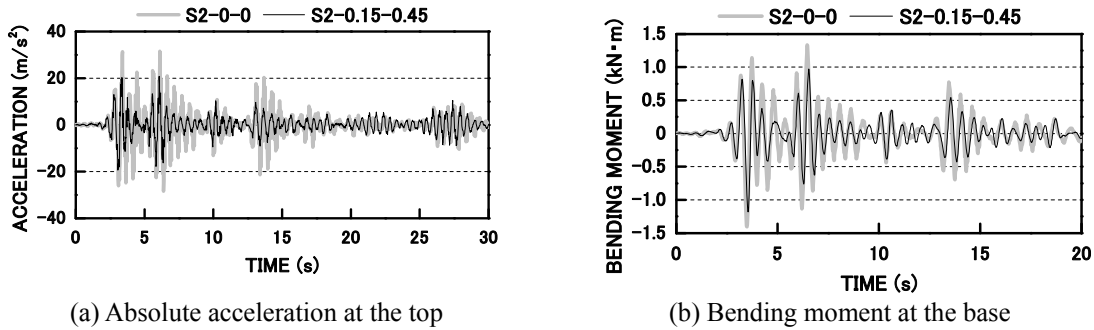


Fig. 5 Time histories of (a) absolute acceleration at the top and (b) bending moment at the base of specimens S2-0-0 and S2-0.15-0.45, subjected to the El Centro 1940 NS 50 waveform

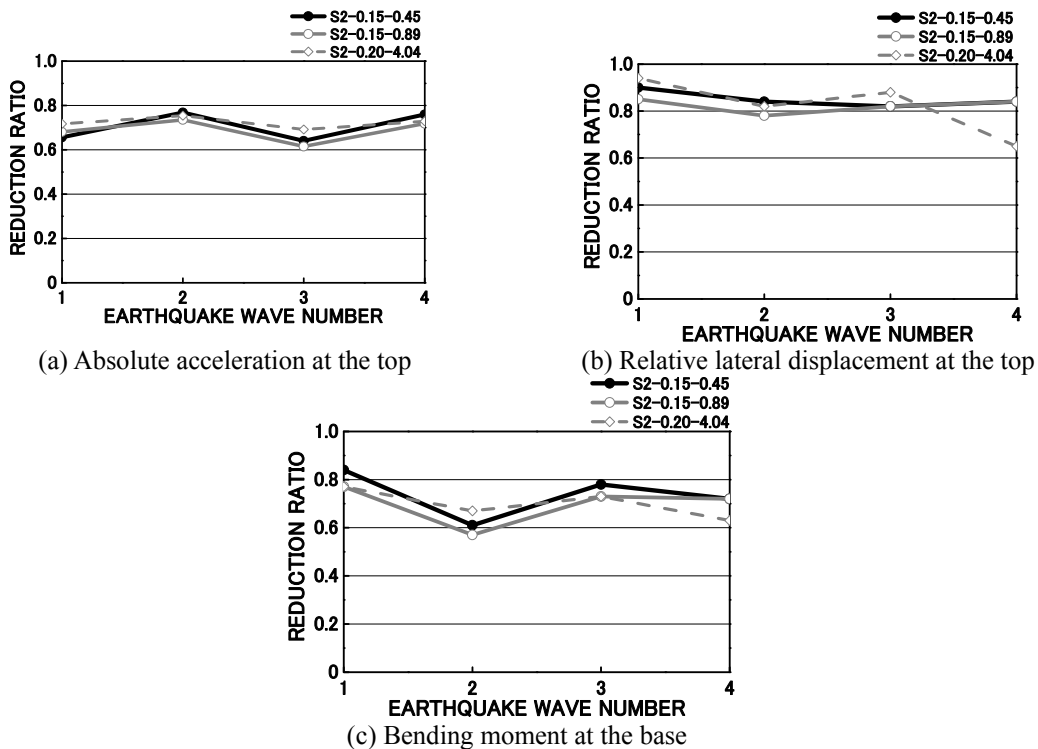


Fig. 6 Reduction ratio for (a) absolute acceleration at the top, (b) relative lateral displacement at the top, and (c) bending moment at the base

### 3.2 Experimental results

Fig. 4 shows the acceleration response spectrum measured at the top of the four specimens during vibration testing with a constant sinusoidal input at 1 to 20 Hz. The first (fundamental) resonance period is at about 0.496 s for all specimens. The second resonance period corresponds to a higher vibration mode.

Figs. 5(a) and (b) show the time histories of the absolute acceleration at the specimen top and

the bending moment at the specimen base, respectively, for S2-0-0-0 and S2-0.15-0.45, subjected to the El Centro 1940 NS 50 waveform.

The effectiveness of the vibration control device is evaluated in terms of the ratios of the maximum acceleration and relative transverse displacement at the top of the specimen, and the bending moment and transverse shear stain at the base. The reduction ratio is defined as the ratio of the maximum response of the specimens with the vibration control device to that without the device. Figs. 6(a)-(c) show the reduction ratios for absolute acceleration, relative transverse displacement and bending moment, respectively. The horizontal axis indicates the earthquake waveform being applied to the shaker table, and the numbers correspond to those shown in Table 3. Although the reduction ratios depend on the particular earthquake, it is clear that the vibration control device is capable of reducing the maximum responses to 60~90 % of their original values.

## 4. Comparison between experimental and numerical results

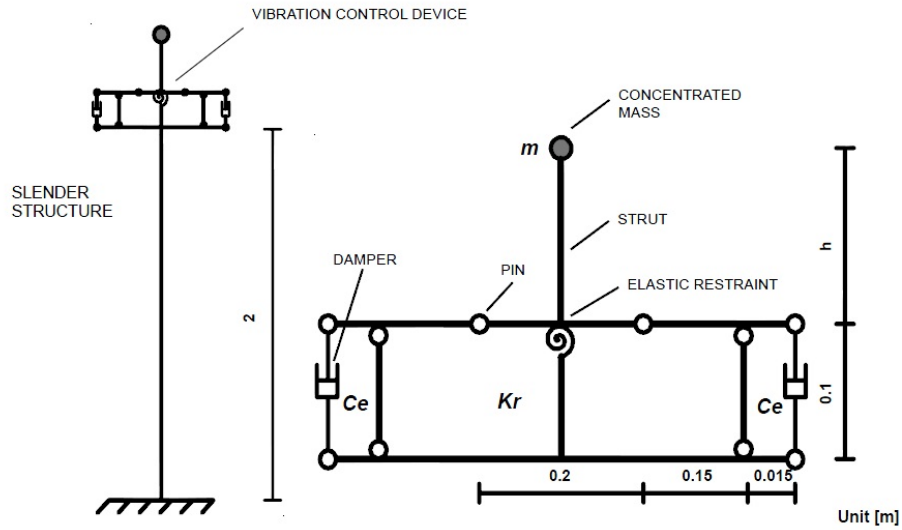
### 4.1 Computational method

In the preceding section, the effectiveness of the proposed device was demonstrated experimentally by subjecting a test specimen to the recorded waveforms of strong earthquakes. However, for a more comprehensive evaluation of the device performance, numerical simulations were carried out using the FEM code SNAP. Fig. 7(a) shows an overview of the computational model used in the present study. Fig. 7(b) shows the details of the vibration control device model.

The computational method involves a nonlinear dynamic analysis, dividing the specimen into 100 beam elements. The rigidity of the urethane elastic restraint is expressed in terms of a rotational rigidity  $K_r$  in the computational model. The values of  $K_r$  and the damping coefficient  $C_e$  of the dampers are determined using the following approximate method, because of restriction from the ability of shaker table for long period of the vibration control device. First,  $K_r$  is determined such that the period of second vibration mode  $T_{EX}$  for the specimen with the vibration control device agrees with the period of second vibration mode  $T_{SNAP}$  obtained from the computation model using SNAP, as shown in Fig. 8. Next,  $C_e$  for the damper is determined such that the experimentally obtained damping constant  $h_{EX}$  is equal to the numerically obtained value  $h_{SNAP}$  for vibration control device alone. It is assumed that the damping constant is independent of vibration mode, i.e.,  $h_i = h_1$ .

### 4.2 Results

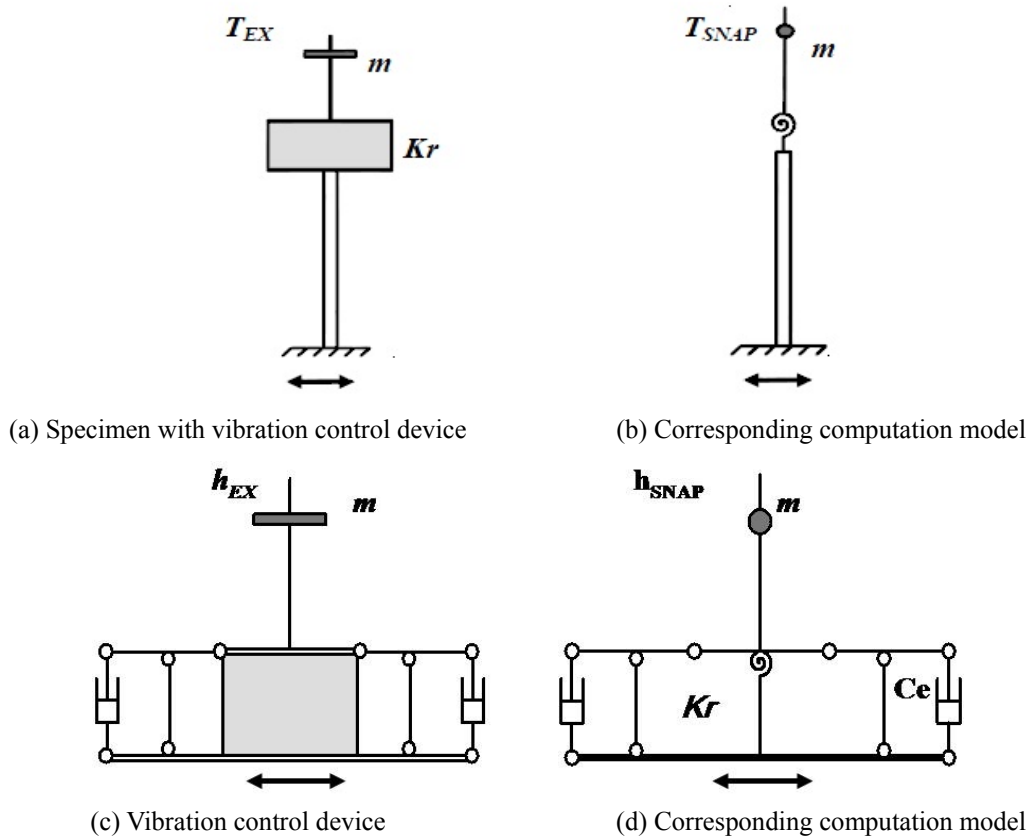
Fig. 9 shows a comparison between the experimental and numerical results for the time history of the absolute acceleration at the top of S2-0.15-0.45, subjected to the El Centro 1940 NS 50 waveform, and Fig. 10 shows the corresponding relative displacement. Fig. 11 compares the experimental and numerical results for the reduction ratios for the absolute acceleration, relative displacement, bending moment and shear strain. Again, the horizontal axis indicates the earthquake index. From the charts, it can be seen that there is reasonably good agreement between the experimental and computational results.



(a) Overall structure

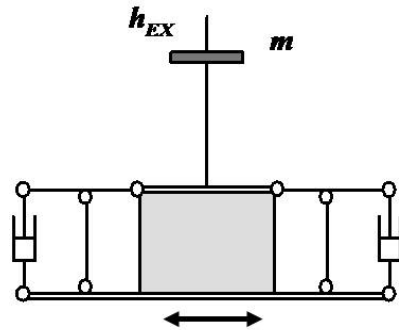
(b) Vibration control device

Fig. 7 Computational model for SNAP simulation: (a) overall structure and (b) vibration control device

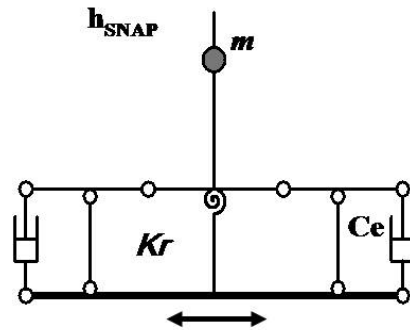


(a) Specimen with vibration control device

(b) Corresponding computation model



(c) Vibration control device



(d) Corresponding computation model

Fig. 8 Modeling setup for vibration control device: (a) specimen with vibration control device, (b) corresponding computation model, (c) vibration control device and (d) corresponding computation model

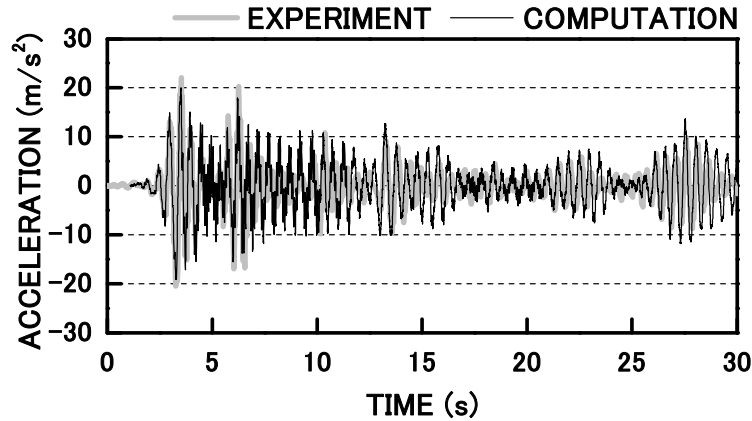


Fig. 9 Absolute acceleration at the top of specimen S2-0.15-0.45, subjected to the El Centro 1940 NS 50 waveform

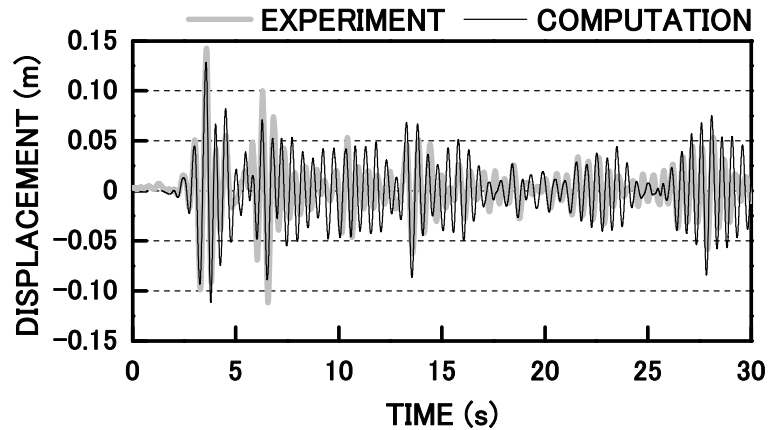


Fig. 10 Relative displacement at the top of specimen S2-0.15-0.45, subjected to the El Centro 1940 NS 50 waveform

## 5. Application to tall steel chimney

In the preceding sections, the effectiveness of the proposed vibration control device was demonstrated both experimentally and numerically. We next numerically simulate its application to a realistic slender structure, which is a tall steel chimney.

### 5.1 Computation model

We consider a steel chimney with a height of 100 m, as illustrated in Fig. 12. The external diameters of the tapered circular cross section are 8.6 m at the base and 5.25 m at the top. The material used is SS400. Young's modulus  $E$  is  $2.05 \times 10^{11}$  N/m<sup>2</sup>, Poisson's ratio is 0.3, and the total mass is  $302 \times 10^3$  kg. Again, the computation method uses SNAP and the chimney is divided into 100 beam elements. Details of the computation model are shown in Fig. 13. To investigate the influence of the rotational rigidity  $Kr$ , the damping coefficient  $Ce$  of the damper, and the

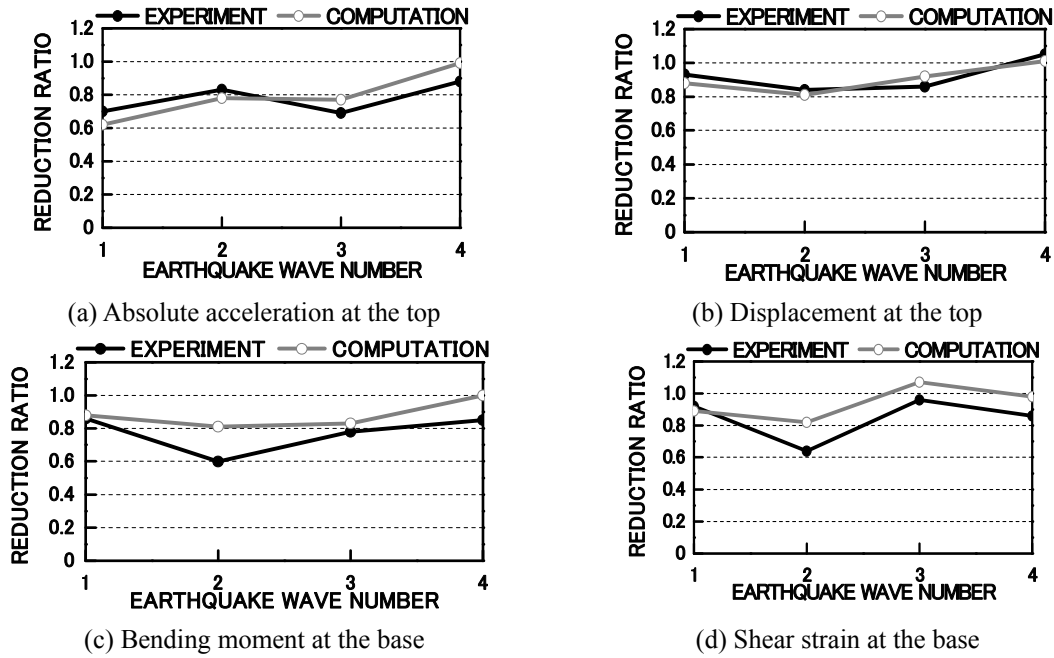


Fig. 11 Reduction ratio for specimen S2-0.15-0.45: (a) absolute acceleration at the top, (b) displacement at the top, (c) bending moment at the base and (d) shear strain at the base

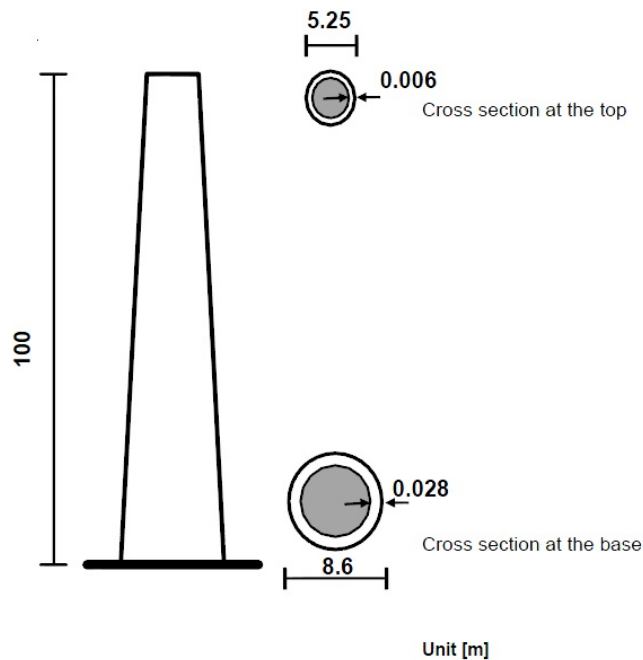


Fig. 12 Dimensions of numerical model of steel chimney

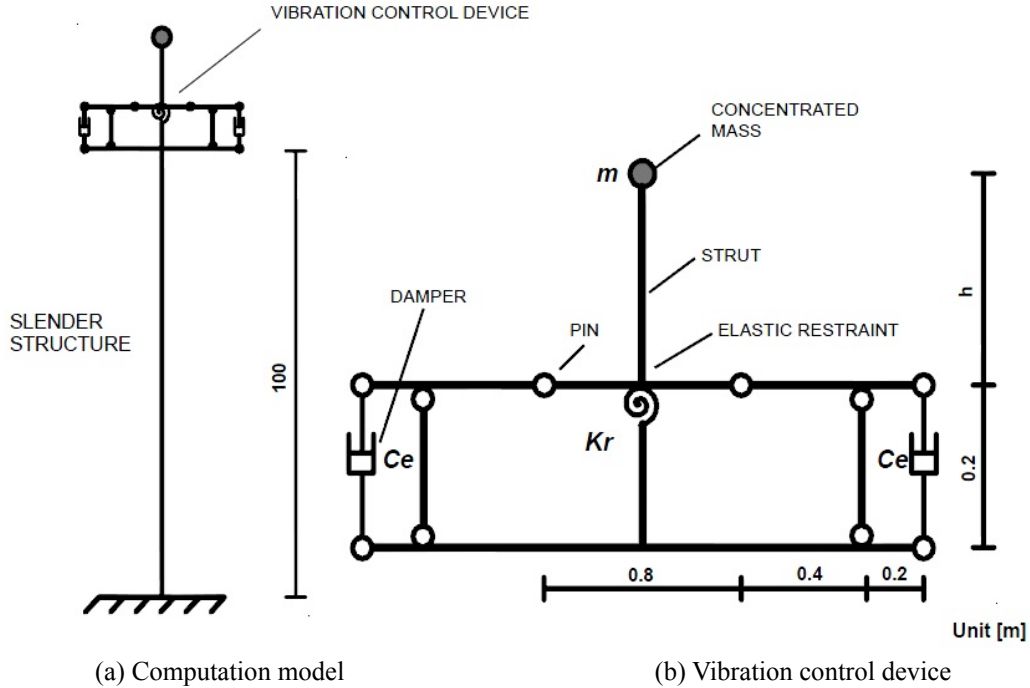


Fig. 13 SNAP computation model of tall steel chimney: (a) overall structure and (b) vibration control device

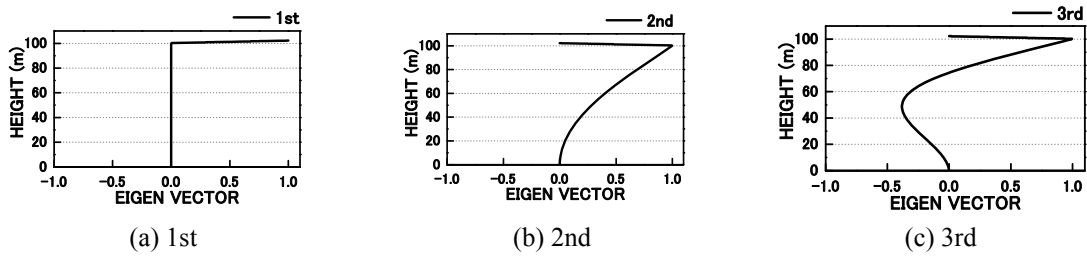


Fig. 14 Eigen modes with vibration control device: (a) 1st , (b) 2nd and (c) 3rd ( $K_r=1.0$  kN·m/rad,  $m=3,000$  kg)

magnitude of the compact mass  $m$  on the effectiveness of vibration control, the following values for these parameters are used:

$$K_r = 1, 10, 100 \text{ kN}\cdot\text{m/rad}$$

$$C_e = 1, 5, 10 \text{ MN/m/s}$$

$$m = 3,000, 6,000, 9,000 \text{ kg}$$

The height,  $h$ , of the compact mass measured from the surface of the elastic restraint is 2 m in the reference state. However, this height is adjusted in order to maintain the natural vibration period for different values of  $K_r$ . The mass  $m$  above corresponds to 1, 2 and 3% of the total mass of the

chimney.

The height of the compact mass is determined such that the second vibration mode of the chimney with the vibration control device attached is the same as the first vibration mode for the chimney alone. Table 4 indicates the natural periods corresponding to various values of  $Kr$ . Fig. 14 shows the eigenfunctions for the chimney with the vibration control device for  $m=3,000$  kg and  $Kr=1.0$  kN·m/rad. For the second mode, the movement of the vibration control device is seen to perfectly oppose that of the chimney.

Table 4 Natural periods without and with vibration control for different rotational rigidity  $K_r$

$K_r$ (kNm/rad)	Natural periods (s)							
	without vibration control		with vibration control					
			Compact mass 3,000 kg		Compact mass 6,000 kg		Compact mass 9,000 kg	
1st	2nd	1st	2nd	1st	2nd	1st	2nd	
1			21.77	0.740	30.78	0.740	37.70	0.740
10	0.740	0.193	6.89	0.740	9.74	0.740	11.93	0.740
100			3.82	0.739	5.40	0.739	6.61	0.739

Table 5 Reduction ratios for absolute acceleration at the top due to vibration control with  $m=9,000$  kg

$K_r$ (kNm/rad)	$C_e$ (MN/m/s)	Reduction ratio for each earthquake excitation						
		1	2	3	4	5	6	7
		El Centro 1940 NS 50	El Centro 1940 NS 70	JMA Kobe NS 50	JMA Kobe NS 75	JMA Kobe NS 100	Noto Peninsula EW 50	Tomakomai NS 50
1	1	0.91	0.91	0.86	0.87	0.86	0.80	0.75
	5	0.74	0.74	0.79	0.80	0.79	0.62	0.48
	10	0.68	0.68	0.79	0.80	0.79	0.53	0.42
10	1	0.91	0.91	0.86	0.87	0.86	0.80	0.75
	5	0.74	0.74	0.79	0.80	0.79	0.62	0.48
	10	0.68	0.68	0.79	0.80	0.79	0.53	0.42
100	1	0.95	0.95	0.95	0.96	0.95	0.94	0.88
	5	0.86	0.86	0.79	0.80	0.79	0.68	0.63
	10	0.78	0.78	0.78	0.79	0.78	0.64	0.51

## 5.2 Results

From the numerical computation results, the following conclusions are obtained.

- (1) For  $C_e=0.1$ , there is no vibration control effect.
- (2) The magnitude of  $Kr$  does not affect the degree of vibration control.
- (3) When  $C_e$  and/or  $m$  become large, the vibration control effect increases.

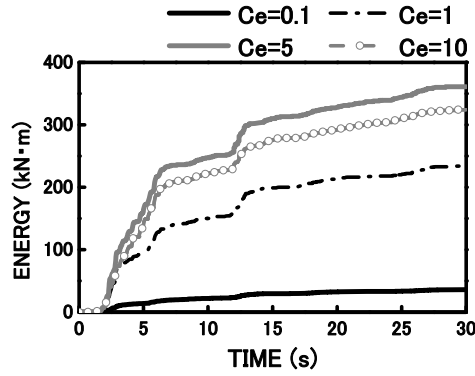


Fig. 15 Time histories of energy produced by dampers in vibration control device with  $K_r=1$  kN·m/rad,  $m=9,000$  kg, and different values of  $C_e$ , subjected to the El Centro 1940 NS 75 waveform

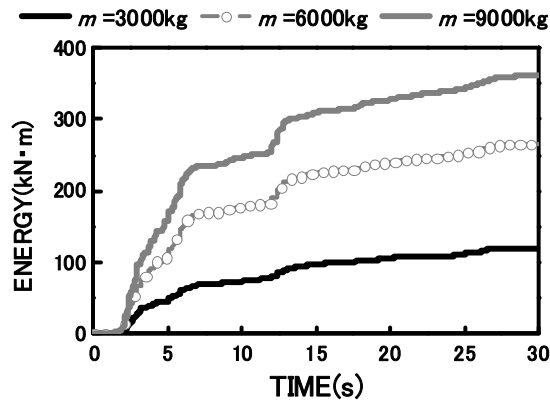


Fig. 16 Time histories of energy produced by dampers in vibration control device with  $K_r=1$  kN·m/rad,  $C_e=5$  MN/m/s and different values of  $m$ , subjected to the El Centro 1940 NS 75 waveform

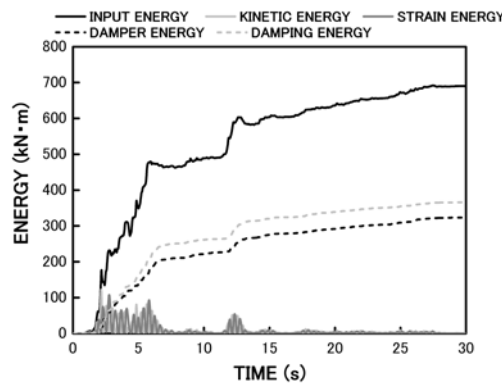


Fig. 17 Time histories of all energy components for chimney with vibration control device with  $K_r=1$  kN/m/rad,  $C_e=10$ , and  $m=9,000$  kg, subjected to the El Centro NS 75 waveform

(4) The enhancement of vibration control by increasing  $C_e$  occurs for all of the earthquake waveforms tested.

Table 5 shows the reduction ratio for the absolute acceleration at the top of the chimney for a vibration control device with a compact mass of  $m=9,000$  kg, subject to seven kinds of earthquake waveforms. The final term in the earthquake labels indicates the normalized magnitude of the maximum velocity. Similarly, Table 6 shows the reduction ratio for the bending moment at the base for the same vibration control device.

Thus, the effectiveness of the proposed vibration control device has been demonstrated for the case of a tall chimney subjected to strong earthquake waves with normalized maximum velocities of 0.50, 0.75 and 1.0 m/s. Fig. 15 shows the time histories of the energy produced by the dampers for a vibration control device with  $m=9,000$  kg,  $Kr=1$  kN·m/rad, and different values of  $C_e$ , when subjected to the El Centro 1940 NS 75 waveform. It can be seen that the optimum performance is achieved for  $C_e=5$ . Fig. 16 shows similar plots for  $C_e=5$  and different values of  $m$ , where it can be seen that the energy produced by the dampers increases with  $m$ . Finally, Fig. 17 shows the time histories of all energy components for  $Kr=1$  kN·m/rad,  $C_e=10$  MN/m/s, and  $m=9,000$  kg, again for the El Centro 1940 NS 75 waveform. The input energy changes mainly to the damper energy produced by the vibration control device and the damping energy due to the vibration of the structure. The damper is very important role for the vibration control of the slender structure.

Thus, effective vibration control can be achieved for a tall chimney during an extremely strong earthquake with a maximum velocity of 1 m/s using a simple device whose weight is only 3% of the weight of the chimney.

## 6. Analytical method

In the preceding sections, the numerical computations were based on the FEM code SNAP. In this section, we consider a general analytical method which is applicable to arbitrary slender structures with abrupt rigidity variations.

Transverse vibrations of slender structures are mainly governed by bending. The equation of transverse motion under the influence of ground motion at the base is

Table 6 Reduction ratios for bending moment at the base due to vibration control with  $m=9,000$  kg

Kr (kNm/rad)	Ce (MN/m/s)	Reduction ratio for each earthquake excitation						
		1	2	3	4	5	6	7
		El Centro 1940 NS 50	El Centro 1940 NS 70	JMA Kobe NS 50	JMA Kobe NS 75	JMA Kobe NS 100	Noto Peninsula EW 50	Tomakomai NS 50
1	1	0.85	0.85	0.91	0.91	0.91	0.75	0.73
	5	0.69	0.69	0.90	0.90	0.90	0.60	0.61
	10	0.71	0.71	0.95	0.95	0.95	0.66	0.61
10	1	0.85	0.85	0.91	0.91	0.91	0.75	0.73
	5	0.69	0.69	0.90	0.90	0.90	0.60	0.61
	10	0.71	0.71	0.95	0.95	0.95	0.66	0.61
100	1	0.93	0.93	0.96	0.96	0.96	0.90	0.90
	5	0.77	0.77	0.88	0.88	0.88	0.68	0.63
	10	0.69	0.69	0.87	0.87	0.87	0.58	0.60

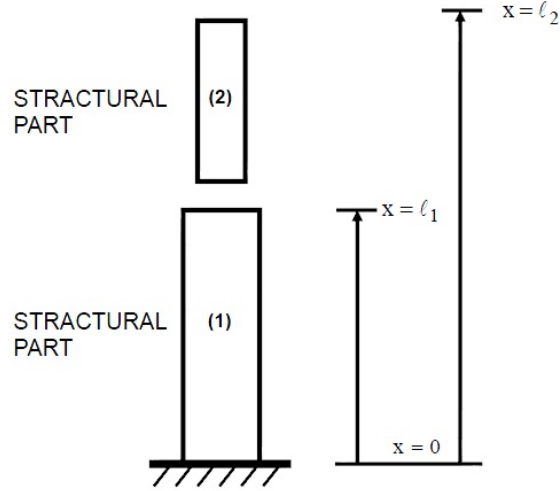


Fig. 18 Schematic illustration of slender structure consisting of two structural parts

$$m\ddot{v} + c\dot{v} + (EIv'')'' = -m\ddot{v}_0, \quad (1)$$

where  $\ddot{v}_0$  is the transverse acceleration at the base due to the earthquake,  $v$  is the relative transverse displacement,  $m$  is the mass per unit length,  $c$  is the damping coefficient and  $EI$  is the bending rigidity. The dashes and dots indicate differentials with respect to the axial direction  $x$  and time  $t$ , respectively.

In order to formulate a general theory which is applicable to arbitrary slender structures with rigidity variations, such structures are regarded as an assemblage of uniform structural parts with constant bending rigidity and constant mass. The overall behavior of the structure is determined by combining the equations of motion for each of these parts, assuming continuity of the conditions across the joints between parts.

The well-known equation for the transverse free vibration of a structural part with a uniform cross section is

$$m\ddot{v} + EIv'''' = 0. \quad (2)$$

Expressing the transverse displacement  $v$  in terms of  $x$  and  $t$ , the solution for the displacement component  $\bar{v}(x)$  becomes

$$\bar{v} = C_1 \cosh(kx) + C_2 \sinh(kx) + C_3 \cos(kx) + C_4 \sin(kx), \quad (3)$$

where  $C_1$  to  $C_4$  are arbitrary constants and  $k^4$  is defined as

$$k^4 = \frac{m\omega^2}{EI}. \quad (4)$$

For simplicity, we consider a slender structure consisting of two structural parts with uniform

properties, as shown in Fig. 18. For parts (1) and (2), the constant  $k$  is expressed as  $k_1$  and  $k_2$ , respectively. Since for the same vibration mode, the natural frequency  $\omega$  of the whole structure must be the same for each part, Eq. (4) gives

$$\omega = C_{01} k_1^2 = C_{02} k_2^2, \quad (5)$$

where the bending wave velocity  $C_{0i}$  for the  $i$ -th structural part is defined as

$$C_{0i}^2 = \frac{EI^{(i)}}{m} \quad (\text{for } i=1,2). \quad (6)$$

The velocity ratio  $\alpha_i$  for the  $i$ -th mode is defined as

$$\alpha_i = \sqrt{\frac{C_{01}}{C_{0i}}}, \quad (7)$$

where  $C_{01}$  is the bending wave velocity for a reference part, which is taken to be part (1) for simplicity. Thus

$$k_i = \alpha_i k_1 \quad (\text{for } i=1, \dots, n), \quad (8)$$

where  $\alpha_1 = 1.0$ . Hence, Eq. (3) for the  $i$ -th structural part may be written as

$$\bar{v}^{(i)} = C_1 \cosh(\alpha_i k_1 x) + C_2 \sinh(\alpha_i k_1 x) + C_3 \cos(\alpha_i k_1 x) + C_4 \sin(\alpha_i k_1 x) \quad (\text{for } i=1, 2). \quad (9)$$

The boundary conditions for this structure are

$$\bar{v}^{(1)} = 0 \quad \text{at } x = 0, \quad (10)$$

$$\bar{v}'^{(1)} = 0 \quad \text{at } x = 0, \quad (11)$$

representing the clamped condition at the base and

$$-EI \bar{v}''^{(2)} = 0 \quad \text{at } x = \ell_2, \quad (12)$$

$$-EI \bar{v}'''^{(2)} = 0 \quad \text{at } x = \ell_2, \quad (13)$$

representing the free condition at the top. Furthermore, the continuity conditions for displacement, rotation, bending moment and shear force at the adjoining point are

$$\bar{v}^{(1)} = \bar{v}^{(2)} \quad \text{at } x = \ell_1, \quad (14)$$

$$\bar{v}'^{(1)} = \bar{v}'^{(2)} \quad \text{at } x = \ell_1, \quad (15)$$

$$-EI \bar{v}'' = -EI \bar{v}'' \quad \text{at } x = \ell_1, \quad (16)$$

$$-EI \bar{v}''' = -EI \bar{v}''' \quad \text{at } x = \ell_1, \quad (17)$$

where the bending moment  $M^{(i)}$  and transverse shear force  $Q^{(i)}$  for the  $i$ -th structural part are expressed as  $M^{(i)} = -EI v''^{(i)}$  and  $Q^{(i)} = -EI v'''^{(i)}$ , respectively.

From Eq. (9), there are a total of eight arbitrary constants for the two structural parts. From Eqs. (10) to (13) and (14) to (17), there are also a total of eight boundary conditions and continuity conditions.

Thus, we obtain homogeneous equations coupled for  $C_1^{(1)} \sim C_4^{(1)}$  and  $C_1^{(2)} \sim C_4^{(2)}$ , as given in Appendix I.

$$[A] \begin{Bmatrix} C_1^{(1)} \\ \vdots \\ C_4^{(1)} \\ C_1^{(2)} \\ \vdots \\ C_4^{(2)} \end{Bmatrix} = 0, \quad (18)$$

where  $[A]$  is an  $8 \times 8$  square matrix. The natural frequencies  $\omega_i$  are obtained by setting the determinant of the coefficient matrix  $[A]$  to zero. For a structure consisting of many parts, continuity conditions must be prepared for each joining point.

A vibration control device set on top of a slender structure is subject to an elastic restraint at its base. There is a very abrupt discontinuity between the bending rigidity of the structure and the device. Therefore, the above method based on continuity across joints is not valid in such a situation. From the expression for the bending moment  $M$ , the relationship between the bending rigidity  $EI$  and elastic restraint  $R$  for bending is given by

$$M = -EI v'' = R v'. \quad (19)$$

For the current vibration control device,  $R$  can be approximately expressed as  $R = \frac{EI}{h_o}$ , corresponding to bending deformation of the urethane elastic restraint, where  $h_o$ ,  $I$  and  $E$  are the thickness, principal moment of inertia, and Young modulus of the urethane, respectively.

Hence, the rotation  $v'$  is expressed by

$$v' = -\frac{EI}{R} v''. \quad (20)$$

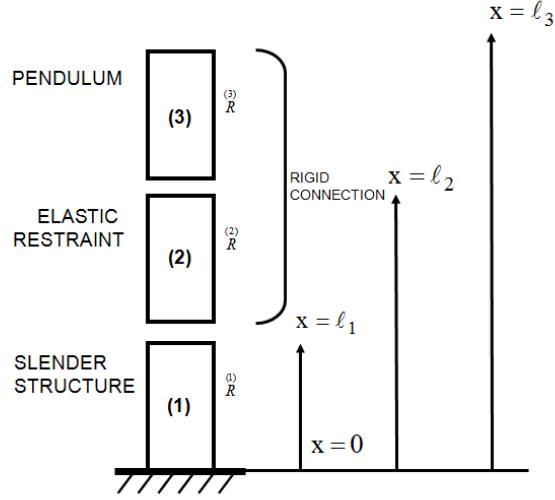


Fig. 19 Analytical model consisting of slender structure (1), elastic restraint (2) and pendulum (3)

The rotations  $v^{(1)}$  and  $v^{(2)}$  for adjoining structural parts (1) and (2) can then be explicitly written as

$$v^{(1)} = -\frac{EI^{(1)}}{R} v''^{(1)}, \quad (21)$$

$$v^{(2)} = -\frac{EI^{(2)}}{R} v''^{(2)}. \quad (22)$$

The continuity conditions for the rotation and bending moment corresponding to Eqs. (15) and (16), respectively, are modified as

$$-\frac{EI^{(1)}}{R} \bar{v}''^{(1)} = -\frac{EI^{(2)}}{R} \bar{v}''^{(2)} \quad \text{at } x = \ell_1, \quad (23)$$

$$-\frac{EI^{(1)}}{R} \bar{v}'^{(1)} = -\frac{EI^{(2)}}{R} \bar{v}'^{(2)} \quad \text{at } x = \ell_1. \quad (24)$$

Thus, for slender structures with an abrupt change in bending rigidity, the divergence in the numerical computations may be prevented by the use of the elastic restraint.

We now apply this analytical method to the proposed vibration control device. In the analytical model, the device is divided into two structural parts: the elastic restraint and the pendulum, labeled as (2) and (3), respectively, in Fig. 19. The slender structure is labeled as (1). Since parts

(2) and (3) are rigidly connected, their rotational rigidities  $R^{(2)}$  and  $R^{(3)}$  are the same. The three structural parts have a total of twelve arbitrary constants (four each). For part (1), the boundary conditions on the base at  $x=0$  are given by Eqs. (10) and (11). The continuity conditions between parts (1) and (2) at  $x=\ell_1$  are

$$\bar{v}^{(1)} = \bar{v}^{(2)} \quad \text{at } x = \ell_1, \quad (25)$$

$$-\frac{EI^{(1)}}{R^{(1)}} \bar{v}''^{(1)} = -\frac{EI^{(2)}}{R^{(2)}} \bar{v}''^{(2)} \quad \text{at } x = \ell_1, \quad (26)$$

$$-R^{(1)(1)} \bar{v}'^{(1)} = -R^{(2)(2)} \bar{v}'^{(2)} \quad \text{at } x = \ell_1, \quad (27)$$

$$-EI^{(1)(1)} \bar{v}'''^{(1)} = -EI^{(2)(2)} \bar{v}'''^{(2)} \quad \text{at } x = \ell_1. \quad (28)$$

Similarly, the continuity conditions between parts (2) and (3) at  $x = \ell_2$  are

$$\bar{v}^{(2)} = \bar{v}^{(3)} \quad \text{at } x = \ell_2, \quad (29)$$

$$-\frac{EI^{(2)}}{R^{(2)}} \bar{v}''^{(2)} = -\frac{EI^{(3)}}{R^{(3)}} \bar{v}''^{(3)} \quad \text{at } x = \ell_2, \quad (30)$$

$$-R^{(2)(2)} \bar{v}'^{(2)} = -R^{(3)(3)} \bar{v}'^{(3)} \quad \text{at } x = \ell_2, \quad (31)$$

$$-EI^{(2)(2)} \bar{v}'''^{(2)} = -EI^{(3)(3)} \bar{v}'''^{(3)} \quad \text{at } x = \ell_2. \quad (32)$$

Finally, the boundary conditions at the top at  $x = \ell_3$  are

$$-EI^{(3)(3)} \bar{v}''^{(3)} = 0 \quad \text{at } x = \ell_3, \quad (33)$$

$$-EI^{(3)(3)} \bar{v}'''^{(3)} = 0 \quad \text{at } x = \ell_3. \quad (34)$$

Thus, we have the following homogeneous equations for 12 unknown arbitrary constants

$$[A]\{C\} = 0, \quad (35)$$

where the coefficient matrix  $[A]$  is a  $12 \times 12$  square matrix and  $\{C\}$  is a column matrix with 12 rows. These matrices are described in detail in Appendix II. The natural frequencies  $\omega_i$  for the slender structure with the vibration control device can be easily determined from the eigenvalues of Eq. (35).

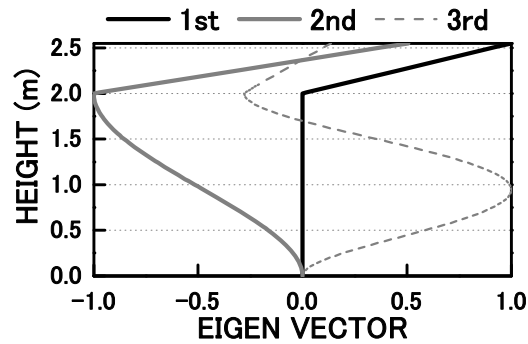


Fig. 20 Eigenfunctions for different vibration modes

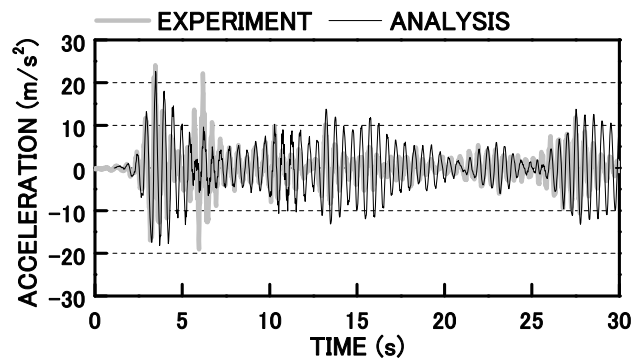


Fig. 21 Analytical and experimental results for time histories of absolute acceleration at the top of specimen S2-0.15-0.89, subjected to the El Centro 1940 NS waveform normalized to a maximum velocity of 0.5 m/s

Table 7 Natural vibration periods for specimen S2-0.15-0.89 for comparison between experiment and analysis

Mode	Natural period (s)		Ratio (2)/(1)
	(1) Analysis	(2) Experiment	
1st	307.539	N/A	N/A
2nd	0.497	0.496	1.00
3rd	0.071	0.080	1.13

## 7. Evaluation of the proposed general analytical method

The analytical method proposed here is evaluated by comparing the analytical and experimental results. For simplicity, the analytical method for the dynamic response is based on modal analysis.

Table 7 shows a comparison between the analytical and experimental results for the natural periods of specimen S2-0.15-0.89, and Fig. 20 shows the eigenfunctions obtained from the analytical results. The eigenfunction for the second vibration mode indicates that structural parts

Table 8 Comparison between analytical and experimental results

No	Earthquake	Maximum response	Analysis			Experiment			Analysis/ Experiment		
			(1) without device	(2) with device	(5) Reduction ratio (2)/(1)	(3) without device	(4) with device	(6) Reduction ratio (4)/(3)	(1)/(3)	(2)/(4)	(5)/(6)
1	El Centro 1940 NS 50	Absolute acceleration (m/s <sup>2</sup> )	28.70	22.84	0.80	31.56	22.08	0.70	0.91	1.03	1.14
		Relative transverse displacement (mm)	153.07	132.66	0.87	153.40	143.00	0.93	1.00	0.93	0.94
2	JMA Kobe NS 50	Absolute acceleration (m/s <sup>2</sup> )	27.94	22.97	0.82	34.10	28.24	0.83	0.82	0.81	0.99
		Relative transverse displacement (mm)	171.82	145.77	0.85	167.80	141.00	0.84	1.02	1.03	1.01
3	Noto Peninsula EW 50	Absolute acceleration (m/s <sup>2</sup> )	33.43	21.13	0.63	32.24	22.22	0.69	1.04	0.95	0.91
		Relative transverse displacement (mm)	112.89	99.68	0.88	100.40	86.20	0.86	1.12	1.16	1.02
4	Tomakomai NS 50	Absolute acceleration (m/s <sup>2</sup> )	6.76	5.42	0.80	6.69	5.91	0.88	1.01	0.92	0.91
		Relative transverse displacement (mm)	37.65	34.20	0.91	33.80	35.40	1.05	1.11	0.97	0.87

(2) and (3), corresponding to the vibration control device, move in the opposite direction to the slender structure (1). Fig. 21 shows a comparison of the time histories of the absolute acceleration at the top of specimen S2-0.15-0.89, subjected to the El Centro 1940 NS 50 waveform. The analytical results indicate excellent agreement with the experimental one. Table 8 compares the analytical and experimental results for the maximum response of the absolute acceleration and the relative transverse displacement for specimens with and without the vibration control device, subjected to four different earthquake waveforms normalized to a maximum velocity of 0.5 m/s. The ratios shown on the right-hand side of this table indicate good agreement between the analytical and experimental results, both with and without the device.

## 8. Conclusions

A new vibration control device for slender structures has been proposed to prevent collapse of such structures during strong earthquakes. The effectiveness of the device has been demonstrated

both experimentally, using a small-scale laboratory model, and through numerical computations. The performance of such a device in real-world applications has also been evaluated by modeling a tall steel chimney.

In addition, a new general method has been developed for transverse free vibration analysis of slender structures with abrupt rigidity variations. This is based on the concept of transforming rotational rigidity into continuity conditions for the rotation and bending moment. The effectiveness of this method was demonstrated by comparison with the experimental results.

Finally, we consider the limitations of the proposed vibration control device, which is based on the fundamental vibration frequency of slender structures. Since, during large earthquakes, the mechanical behavior of a structure can change from elastic to inelastic, the effectiveness of such an approach may be reduced. However, slender structures normally have a very high aspect ratio and their collapse is a result of the overturning moment. They are generally designed to be elastic because they contain few structural members. For this reason, it is believed that the proposed method of vibration control would be effective over a relatively wide range of conditions.

## Acknowledgments

This research was supported by Grants-in-Aid for Scientific Research in Japan (No. 21560600). We would like to thank T. Honda, a member of staff at the Institute of Disaster and Environmental Science, for her help and useful suggestions.

## References

- Abé, M. and Fujino, Y. (1994), "Dynamic characterization of multiple tuned mass dampers and some design formulas", *Earthq. Eng. Struct. D.*, **23**(8), 813–835.
- Abé, M. (1996), "Semi-active tuned mass dampers for seismic protection of civil structures", *Earthq. Eng. Struct. D.*, **25**(7), 743-749.
- Abé, M. (1996), "Tuned mass dampers for structures with bilinear hysteresis", *J. Eng. Mech.*, **122**(8), 797-800.
- Abé, M. and Igusa, T. (1996), "Semi-active dynamic vibration absorbers for controlling transient response", *J. Sound Vib.*, **198**(5), 547-569.
- Balendra, T., Wang, C.M. and Cheong, H.F. (1995), "Effectiveness of tuned liquid column dampers for vibration control of towers", *Eng. Struct.*, **17**(9), 668-675.
- Boley, B.A. (1963), "On the accuracy of the Bernoulli-Euler theory for beams of variable section", *J. Appl. Mech.*, **30**(3), 373-378.
- Chang, J.C.H. and Soong, T.T. (1980), "Structural control using active tuned mass dampers", *J. Eng. Mech.*, **106**(6), 1091-1098.
- Fujii, K., Tamura, Y., Sato, T. and Wakahara, T. (1990), "Wind-induced vibration of tower and practical applications of tuned sloshing damper", *J. Wind Eng. Ind. Aerod.*, **33**(1-2), 263-272.
- Fujino, Y. and Abé, M. (1993), "Design formulas for tuned mass dampers based on a perturbation technique", *Earthq. Eng. Struct. D.*, **22**(10), 833-854.
- Gerges, R.R. and Vickery, B.J. (2005), "Optimum design of pendulum-type tuned mass damper", *Struct. Des. Tall Spec. Build.*, **14**(4), 353-368.
- Ghosh, A. and Basu, B. (2004), "Seismic vibration control of short period structures using the liquid column damper", *Eng. Struct.*, **26**(2004), 1905-1913.
- Ghosh, A. and Basu, B. (2008), "Seismic vibration control of nonlinear structures using the liquid column

- damper”, *J. Struct. Eng.*, **134**(1), 146-153.
- Gupta, A.K. (1985), “Vibration of tapered beams”, *J. Struct. Div.-ASCE*, **111**(1), 19-36.
- Gupta, A.K. (1986), “Frequency-dependent matrices for tapered beams”, *J. Struct. Eng.-ASCE*, **112**(1), 85-103.
- Igusa, T. and Xu, K. (1994), “Vibration control using multiple tuned mass dampers”, *J. Sound Vib.*, **175**(4), 491-503.
- Johnston, B.G. (1976), *Guide to stability design criteria for metal structures*, Chap. II. Tapered structural members, 3rd Ed., John Wiley & Sons, Inc., New York, N.Y., 330-358.
- Kareem, A. and Kline, S. (1995), “Performance of multiple mass damper under random loading”, *J. Struct. Eng.*, **12**(2), 348-361.
- Kaynia, A.M., Biggs, J.M. and Veneziano, D. (1981), “Seismic effectiveness of tuned mass dampers”, *J. Struct. Div.-ASCE*, **107**(8), 1465-1484.
- Kobori, T., Takahashi, M., Nasu, T., Niwa, N. and Ogasawara, K. (1993), “Seismic response controlled structure with Active Variable Stiffness system”, *Earthq. Eng. Struct. D.*, **22**(11), 925-941.
- Lin, C.C., Lin, G.L. and Wang, J.F. (2010), “Protection of seismic structures using semi-active friction TMD”, *Earthq. Eng. Struct. D.*, **39**(6), 635-659.
- Nagarajaiah, S. and Sonmez, E. (2007), “Structures with semiactive variable stiffness single/multiple tuned mass dampers”, *J. Struct. Eng.*, **133**(1), 67-77.
- Nagarajaiah, S. and Varadarajan, N. (2004), “Short time fourier transform algorithm for wind response control of buildings with variable stiffness TMD”, *Eng. Struct.*, **27**(2005), 431-441.
- Nagarajaiah, S. and Narasimhan, S. (2007), “Seismic control of smart base isolated buildings with new semiactive variable damper”, *Earthq. Eng. Struct. D.*, **36**(6), 729-749.
- Prathap, G. and Varadan, T.K. (1976), “Finite deflection of tapered cantilevers”, *J. Eng. Mech. Div.-ASCE*, **102**(3), 549-552.
- Roffel, A.J., Lourenco, R., Narasimham, S. and Yarusyevych, S. (2011), “Adaptive compensation for detuning in pendulum turned mass dampers”, *J. Struct. Eng.*, **137**(2), 242-251.
- Rohde, F.V. (1953), “Large deflections of cantilever beam with uniformly distributed load”, *Q. Appl. Math.*, **11**, 337.
- Setareh, M., Ritchey, J.K., Murray, T.M., Koo, J.H. and Ahmadian, M. (2007), “Semiactive tuned mass damper for floor vibration control”, *J. Struct. Eng.*, **133**(2), 242-250.
- Sun, J.Q., Jolly, M.R. and Norris, M.A. (1995), “Passive, adaptive and active tuned vibration absorbers – A survey”, *Trans. ASME J. Mech. Des.*, **117**(B), 235-242.
- Takabatake, H. (1990), “Cantilevered and linearly tapered thin-walled members”, *J. Eng. Mech.*, **116**(4), 733-750.
- Takabatake, H. and Mizuki, A. (1995), “Simplified dynamic analysis of slender tapered thin-walled towers with additional mass and rigidity”, *J. Eng. Mech.*, **3**(1), 61-74.
- Takabatake, H. and Satoh, T. (2006), “A simplified analysis and vibration control to super-high-rise buildings”, *Struct. Des. Tall Spec. Build.*, **15**(4), 363-390.
- Takabatake, H. and Ikarashi, F. and Matsuoka, M. (2011), “A simplified analysis of super building structures with setback”, *Earthq. Struct.*, **2**(1), 43-64.
- Tesar, A. (1999), “Tuned vibration control of slender structures”, *Int. J. Numer. Eng.*, **45**(9), 1243-1255.
- Thompson, A.G. (1981), “Optimum tuning and damping of a dynamic vibration absorber applied to a force excited and damped primary system”, *J. Sound Vib.*, **77**(3), 403-415.
- Varadarajan, N. and Nagarajaiah, S. (2004), “Wind response control of building with variable stiffness tuned mass damper using empirical mode demoposition/hilbert transform”, *J. Eng. Mech.*, **130**(4), 451-458.
- Wang, T.M. and Lee, C.H. (1973), “Tapered cantilevers with varying distributed loads”, *J. Eng. Mech. Div.-ASCE*, **99**(4), 919-925.
- Won, A.Y.J., Pires, J.A. and Haroun, M.A. (1996), “Stochastic seismic evaluation of tuned liquid column dampers”, *Earthq. Eng. Struct. D.*, **25**(11), 1259-1274.
- Xu, K. and Igusa, T. (1992), “Dynamic characteristics of multiple substructures with closely spaced frequencies”, *Earthq. Eng. Struct. D.*, **21**(12), 1059-1070.

- Xu, L.H. and Li, Z.X. (2008), "Semi-active multi-step predictive control of structures using MR dampers", *Earthq. Eng. Struct. D.*, **37**(12), 1435-1448.
- Yalla, S.K. and Kareem, A. (2000), "Optimum absorber parameters for tuned liquid column dampers", *J. Struct. Eng.*, **126**(8), 906-915.
- Yamaguchi, H. and Harnpornchai, N. (1993), "Fundamental characteristics of multiple tuned mass dampers for suppressing harmonically forced oscillations", *Earthq. Eng. Struct. D.*, **22**(1), 51-62.
- Zemp, R., Juan, C. de la Llera and Almazán, J.L. (2011), "Tall building vibration control using a TM-MR damper assembly", *Earthq. Eng. Struct. D.*, **40**(3), 339-354.

*IT*

**Appendix I**

Eq. (18) can be written in the explicit form

$$\begin{bmatrix} a_{11} & a_{12} & a_{13} & a_{14} & a_{15} & a_{16} & a_{17} & a_{18} \\ a_{21} & a_{22} & a_{23} & a_{24} & a_{25} & a_{26} & a_{27} & a_{28} \\ a_{31} & a_{32} & a_{33} & a_{34} & a_{35} & a_{36} & a_{37} & a_{38} \\ a_{41} & a_{42} & a_{43} & a_{44} & a_{45} & a_{46} & a_{47} & a_{48} \\ a_{51} & a_{52} & a_{53} & a_{54} & a_{55} & a_{56} & a_{57} & a_{58} \\ a_{61} & a_{62} & a_{63} & a_{64} & a_{65} & a_{66} & a_{67} & a_{68} \\ a_{71} & a_{72} & a_{73} & a_{74} & a_{75} & a_{76} & a_{77} & a_{78} \\ a_{81} & a_{82} & a_{83} & a_{84} & a_{85} & a_{86} & a_{87} & a_{88} \end{bmatrix} \begin{bmatrix} C_1^{(1)} \\ C_2^{(1)} \\ C_3^{(1)} \\ C_4^{(1)} \\ C_1^{(2)} \\ C_2^{(2)} \\ C_3^{(2)} \\ C_4^{(2)} \end{bmatrix} = 0 \quad (\text{A1})$$

where the elements  $a_{ij}$  of the  $8 \times 8$  square matrix are

$$\begin{aligned} a_{11} &= 1; & a_{12} &= 0; & a_{13} &= 1; & a_{14} &= 0; & a_{15} &= 0; & a_{16} &= 0; & a_{17} &= 0; & a_{18} &= 0; \\ a_{21} &= 0; & a_{22} &= 1; & a_{23} &= 0; & a_{24} &= 1; & a_{25} &= 0; & a_{26} &= 0; & a_{27} &= 0; & a_{28} &= 0; \\ a_{31} &= \cosh(k_1 \ell_1); & a_{32} &= \sinh(k_1 \ell_1); & a_{33} &= \cos(k_1 \ell_1); & a_{34} &= \sin(k_1 \ell_1); \\ a_{35} &= -\cosh(\alpha_2 k_1 \ell_1); & a_{36} &= -\sinh(\alpha_2 k_1 \ell_1); & a_{37} &= -\cos(\alpha_2 k_1 \ell_1); & a_{38} &= -\sin(\alpha_2 k_1 \ell_1); \\ a_{41} &= \alpha_1 \sinh(k_1 \ell_1); & a_{42} &= \alpha_1 \cosh(k_1 \ell_1); & a_{43} &= -\alpha_1 \sin(k_1 \ell_1); & a_{44} &= \alpha_1 \cos(k_1 \ell_1); \\ a_{45} &= -\alpha_2 \sinh(\alpha_2 k_1 \ell_1); & a_{46} &= -\alpha_2 \cosh(\alpha_2 k_1 \ell_1); & a_{47} &= \alpha_2 \sin(\alpha_2 k_1 \ell_1); & a_{48} &= -\alpha_2 \cos(\alpha_2 k_1 \ell_1); \\ a_{51} &= \alpha_1^2 \cosh(k_1 \ell_1); & a_{52} &= \alpha_1^2 \sinh(k_1 \ell_1); & a_{53} &= -\alpha_1^2 \cos(k_1 \ell_1); & a_{54} &= -\alpha_1^2 \sin(k_1 \ell_1); \\ a_{55} &= -\beta_1 (\alpha_2)^2 \cosh(\alpha_2 k_1 \ell_1); & a_{56} &= -\beta_1 (\alpha_2)^2 \sinh(\alpha_2 k_1 \ell_1); & a_{57} &= \beta_1 (\alpha_2)^2 \cos(\alpha_2 k_1 \ell_1); \\ a_{58} &= \beta_1 (\alpha_2)^2 \sin(\alpha_2 k_1 \ell_1); \\ a_{61} &= \alpha_1^3 \sinh(k_1 \ell_1); & a_{62} &= \alpha_1^3 \cosh(k_1 \ell_1); & a_{63} &= \alpha_1^3 \sin(k_1 \ell_1); & a_{64} &= -\alpha_1^3 \cos(k_1 \ell_1); \\ a_{65} &= -\beta_1 (\alpha_2)^3 \sinh(\alpha_2 k_1 \ell_1); & a_{66} &= -\beta_1 (\alpha_2)^3 \cosh(\alpha_2 k_1 \ell_1); & a_{67} &= -\beta_1 (\alpha_2)^3 \sin(\alpha_2 k_1 \ell_1); \\ a_{68} &= \beta_1 (\alpha_2)^3 \cos(\alpha_2 k_1 \ell_1); \\ a_{71} &= 0; & a_{72} &= 0; & a_{73} &= 0; & a_{74} &= 0; \\ a_{75} &= \cosh(\alpha_2 k_1 \ell_2); & a_{76} &= \sinh(\alpha_2 k_1 \ell_2); & a_{77} &= -\cos(\alpha_2 k_1 \ell_2); & a_{78} &= -\sin(\alpha_2 k_1 \ell_2); \\ a_{81} &= 0; & a_{82} &= 0; & a_{83} &= 0; & a_{84} &= 0; \\ a_{85} &= \sinh(\alpha_2 k_1 \ell_2); & a_{86} &= \cosh(\alpha_2 k_1 \ell_2); & a_{87} &= \sin(\alpha_2 k_1 \ell_2); & a_{88} &= -\cos(\alpha_2 k_1 \ell_2) \end{aligned}$$

**Appendix II**

The homogeneous equations described by the matrix expression (35) for a slender structure with a vibration control device, as shown in Fig. 19, are expressed as

$$[A] = [a_{ij}] \quad (A2)$$

$$\{C\}^T = \left\{ \begin{matrix} (1) & (1) & (1) & (1) & (2) & (2) & (2) & (2) & (3) & (3) & (3) & (3) \\ C_1 & C_2 & C_3 & C_4 & C_1 & C_2 & C_3 & C_4 & C_1 & C_2 & C_3 & C_4 \end{matrix} \right\} \quad (A3)$$

The matrix  $[A]$  is a  $12 \times 12$  matrix, whose elements are

$$a_{11} = 1; \quad a_{12} = 0; \quad a_{13} = 1; \quad a_{14} = 0; \quad a_{15} = 0; \quad a_{16} = 0; \quad a_{17} = 0; \quad a_{18} = 0;$$

$$a_{19} = 0; \quad a_{10} = 0; \quad a_{111} = 0; \quad a_{112} = 0$$

$$a_{21} = 0; \quad a_{22} = 1; \quad a_{23} = 0; \quad a_{24} = 1; \quad a_{25} = 0; \quad a_{26} = 0; \quad a_{27} = 0; \quad a_{28} = 0;$$

$$a_{29} = 0; \quad a_{210} = 0; \quad a_{211} = 0; \quad a_{212} = 0$$

$$a_{31} = \cosh(\alpha_1 k_1 \ell_1); \quad a_{32} = \sinh(\alpha_1 k_1 \ell_1); \quad a_{33} = \cos(\alpha_1 k_1 \ell_1); \quad a_{34} = \sin(\alpha_1 k_1 \ell_1);$$

$$a_{35} = -\cosh(\alpha_2 k_1 \ell_1); \quad a_{36} = -\sinh(\alpha_2 k_1 \ell_1); \quad a_{37} = -\cos(\alpha_2 k_1 \ell_1); \quad a_{38} = -\sin(\alpha_2 k_1 \ell_1);$$

$$a_{39} = 0; \quad a_{310} = 0; \quad a_{311} = 0; \quad a_{312} = 0$$

$$a_{41} = \frac{(1)}{R} EI (\alpha_1)^2 \cosh(\alpha_1 k_1 \ell_1); \quad a_{42} = \frac{(1)}{R} EI (\alpha_1)^2 \sinh(\alpha_1 k_1 \ell_1); \quad a_{43} = -\frac{(1)}{R} EI (\alpha_1)^2 \cos(\alpha_1 k_1 \ell_1);$$

$$a_{44} = -\frac{(1)}{R} EI (\alpha_1)^2 \sin(\alpha_1 k_1 \ell_1); \quad a_{45} = -\frac{(2)}{R} EI (\alpha_2)^2 \cosh(\alpha_2 k_1 \ell_1); \quad a_{46} = -\frac{(2)}{R} EI (\alpha_2)^2 \sinh(\alpha_2 k_1 \ell_1);$$

$$a_{47} = \frac{(2)}{R} EI (\alpha_2)^2 \cos(\alpha_2 k_1 \ell_1); \quad a_{48} = \frac{(2)}{R} EI (\alpha_2)^2 \sin(\alpha_2 k_1 \ell_1);$$

$$a_{49} = 0; \quad a_{410} = 0; \quad a_{411} = 0; \quad a_{412} = 0$$

$$a_{51} = \frac{(1)}{R} \alpha_1 \sinh(\alpha_1 k_1 \ell_1); \quad a_{52} = \frac{(1)}{R} \alpha_1 \cosh(\alpha_1 k_1 \ell_1); \quad a_{53} = -\frac{(1)}{R} \alpha_1 \sin(\alpha_1 k_1 \ell_1);$$

$$a_{54} = \frac{(1)}{R} \alpha_1 \cos(\alpha_1 k_1 \ell_1); \quad a_{55} = -\frac{(2)}{R} \alpha_2 \sinh(\alpha_2 k_1 \ell_1); \quad a_{56} = -\frac{(2)}{R} \alpha_2 \cosh(\alpha_2 k_1 \ell_1);$$

$$a_{57} = \frac{(2)}{R} \alpha_2 \sin(\alpha_2 k_1 \ell_1); \quad a_{58} = -\frac{(2)}{R} \alpha_2 \cos(\alpha_2 k_1 \ell_1);$$

$$a_{59} = 0; \quad a_{510} = 0; \quad a_{511} = 0; \quad a_{512} = 0$$

$$a_{61} = \alpha_1^3 \sinh(\alpha_1 k_1 \ell_1); \quad a_{62} = \alpha_1^3 \cosh(\alpha_1 k_1 \ell_1); \quad a_{63} = \alpha_1^3 \sin(\alpha_1 k_1 \ell_1); \quad a_{64} = -\alpha_1^3 \cos(\alpha_1 k_1 \ell_1);$$

$$a_{65} = -\beta_1 (\alpha_2)^3 \sinh(\alpha_2 k_1 \ell_1); \quad a_{66} = -\beta_1 (\alpha_2)^3 \cosh(\alpha_2 k_1 \ell_1); \quad a_{67} = -\beta_1 (\alpha_2)^3 \sin(\alpha_2 k_1 \ell_1);$$

$$a_{68} = \beta_1 (\alpha_2)^3 \cos(\alpha_2 k_1 \ell_1);$$

$$a_{69} = 0; \quad a_{610} = 0; \quad a_{611} = 0; \quad a_{612} = 0$$

$$a_{7\ 1} = 0; \quad a_{7\ 2} = 0; \quad a_{7\ 3} = 0; \quad a_{7\ 4} = 0;$$

$$a_{7\ 5} = \cosh(\alpha_2 k_1 \ell_2); \quad a_{7\ 6} = \sinh(\alpha_2 k_1 \ell_2); \quad a_{7\ 7} = \cos(\alpha_2 k_1 \ell_2); \quad a_{7\ 8} = \sin(\alpha_2 k_1 \ell_2);$$

$$a_{7\ 9} = -\cosh(\alpha_3 k_1 \ell_2); \quad a_{7\ 10} = -\sinh(\alpha_3 k_1 \ell_2); \quad a_{7\ 11} = -\cos(\alpha_3 k_1 \ell_2); \quad a_{7\ 12} = -\sin(\alpha_3 k_1 \ell_2)$$

$$a_{8\ 1} = 0; \quad a_{8\ 2} = 0; \quad a_{8\ 3} = 0; \quad a_{8\ 4} = 0;$$

$$a_{8\ 5} = \frac{EI}{R} (\alpha_2)^2 \cosh(\alpha_2 k_1 \ell_2); \quad a_{8\ 6} = \frac{EI}{R} (\alpha_2)^2 \sinh(\alpha_2 k_1 \ell_2); \quad a_{8\ 7} = -\frac{EI}{R} (\alpha_2)^2 \cos(\alpha_2 k_1 \ell_2);$$

$$a_{8\ 8} = -\frac{EI}{R} (\alpha_2)^2 \sin(\alpha_2 k_1 \ell_2); \quad a_{8\ 9} = -\frac{EI}{R} (\alpha_3)^2 \cosh(\alpha_3 k_1 \ell_2); \quad a_{8\ 10} = -\frac{EI}{R} (\alpha_3)^2 \sinh(\alpha_3 k_1 \ell_2);$$

$$a_{8\ 11} = \frac{EI}{R} (\alpha_3)^2 \cos(\alpha_3 k_1 \ell_2); \quad a_{8\ 12} = \frac{EI}{R} (\alpha_3)^2 \sin(\alpha_3 k_1 \ell_2)$$

$$a_{9\ 1} = 0; \quad a_{9\ 2} = 0; \quad a_{9\ 3} = 0; \quad a_{9\ 4} = 0;$$

$$a_{9\ 5} = R \alpha_2 \sinh(\alpha_2 k_1 \ell_2); \quad a_{9\ 6} = R \alpha_2 \cosh(\alpha_2 k_1 \ell_2); \quad a_{9\ 7} = -R \alpha_2 \sin(\alpha_2 k_1 \ell_2);$$

$$a_{9\ 8} = R \alpha_2 \cos(\alpha_2 k_1 \ell_2); \quad a_{9\ 9} = -R \alpha_3 \sinh(\alpha_3 k_1 \ell_2); \quad a_{9\ 10} = -R \alpha_3 \cosh(\alpha_3 k_1 \ell_2);$$

$$a_{9\ 11} = R \alpha_3 \sin(\alpha_3 k_1 \ell_2); \quad a_{9\ 12} = -R \alpha_3 \cos(\alpha_3 k_1 \ell_2)$$

$$a_{10\ 1} = 0; \quad a_{10\ 2} = 0; \quad a_{10\ 3} = 0; \quad a_{10\ 4} = 0;$$

$$a_{10\ 5} = \alpha_2^3 \sinh(\alpha_2 k_1 \ell_2); \quad a_{10\ 6} = \alpha_2^3 \cosh(\alpha_2 k_1 \ell_2); \quad a_{10\ 7} = \alpha_2^3 \sin(\alpha_2 k_1 \ell_2); \quad a_{10\ 8} = -\alpha_2^3 \cos(\alpha_2 k_1 \ell_2);$$

$$a_{10\ 9} = -\beta_2 (\alpha_3)^3 \sinh(\alpha_3 k_1 \ell_2); \quad a_{10\ 10} = -\beta_2 (\alpha_3)^3 \cosh(\alpha_3 k_1 \ell_2);$$

$$a_{10\ 11} = -\beta_2 (\alpha_3)^3 \sin(\alpha_3 k_1 \ell_2); \quad a_{10\ 12} = \beta_2 (\alpha_3)^3 \cos(\alpha_3 k_1 \ell_2)$$

$$a_{11\ 1} = 0; \quad a_{11\ 2} = 0; \quad a_{11\ 3} = 0; \quad a_{11\ 4} = 0; \quad a_{11\ 5} = 0; \quad a_{11\ 6} = 0; \quad a_{11\ 7} = 0; \quad a_{11\ 8} = 0;$$

$$a_{11\ 9} = \cosh(\alpha_2 k_1 \ell_2); \quad a_{11\ 10} = \sinh(\alpha_2 k_1 \ell_2); \quad a_{11\ 11} = -\cos(\alpha_2 k_1 \ell_2); \quad a_{11\ 12} = -\sin(\alpha_2 k_1 \ell_2)$$

$$a_{12\ 1} = 0; \quad a_{12\ 2} = 0; \quad a_{12\ 3} = 0; \quad a_{12\ 4} = 0; \quad a_{12\ 5} = 0; \quad a_{12\ 6} = 0; \quad a_{12\ 7} = 0; \quad a_{12\ 8} = 0;$$

$$a_{12\ 9} = \sinh(\alpha_2 k_1 \ell_2); \quad a_{12\ 10} = \cosh(\alpha_2 k_1 \ell_2); \quad a_{12\ 11} = \sin(\alpha_2 k_1 \ell_2); \quad a_{12\ 12} = -\cos(\alpha_2 k_1 \ell_2)$$